

**Empirical Conversions of Broad-Band Optical and Infrared  
Magnitudes to Monochromatic Continuum Luminosities  
for Active Galactic Nuclei**

S. Kozłowski

Warsaw University Observatory, Al. Ujazdowskie 4, 00-478 Warszawa, Poland  
e-mail: simkoz@astrouw.edu.pl*Received August 15, 2015*

## ABSTRACT

We use public data for 105 783 quasars from The Sloan Digital Sky Survey (SDSS) Data Release 7 (DR7) that include spectral monochromatic luminosities at 5100 Å, 3000 Å, and 1350 Å, and the corresponding observed broad-band *ugriz*, *VRI* (converted), *JHK* and WISE magnitudes, and derive broad-band-to-monochromatic luminosity ratios independent of a cosmological model. The ratios span the redshift range of  $z = 0.1 \div 4.9$  and may serve as a proxy for measuring the bolometric luminosity, broad line region (BLR) radii and/or black hole masses, whenever flux-calibrated spectra are unavailable or the existing spectra have low signal-to-noise ratios. They are provided both in tabular and parametric form.

**Key words:** *Galaxies: active – quasars: general – Techniques: photometric*

**1. Introduction**

Active galactic nuclei (AGNs) owe their tremendous brightness to accretion disks forming around supermassive black holes at their centers. It is presumed that the disk temperature  $T$  falls off with the disk radius  $R$  as  $T \propto R^{-3/4}$  (e.g., Shakura and Sunyaev 1973), giving rise to a wide range of photon energies at a continuous range of wavelengths – a feature known as the “continuum” in observed AGN spectra. This continuum can be described either at particular wavelengths (monochromatic luminosities) or in standard broad-band filters (broad-band luminosities).

Continuum photons, either monochromatic, broad-band, or bolometric, may provide key diagnostics in understanding AGN physics, as they respond to the hard UV ionizing photons. A fraction of these UV photons is partially absorbed by the gas-dust clouds away from the disk, in the broad line region (BLR), and re-emitted in a form of broad emission lines at wavelengths corresponding to certain differences between energy levels in atoms and molecules. The typical distance to the clouds is  $r = c\tau$ , so they reverberate any luminosity changes with time-lags  $\tau$  that

are strongly correlated with the continuum luminosity  $L$  as  $\tau \approx r \propto L^{1/2}$ . This is commonly known as the BLR radius–luminosity relation (*e.g.*, Kaspi *et al.* 2000, 2007, Bentz *et al.* 2009). The implications of this relation are essential in the determination of the central black hole mass  $M_{BH}$  via the virial theorem  $M_{BH} \propto L^{1/2}v^2$ , where  $v$  is the velocity of the BLR gas–dust clouds (*e.g.*, Vestergaard and Peterson 2006). Their velocity is routinely measured from AGN spectra as either full width (of the broad emission line) at its half maximum (FWHM) or dispersion ( $\sigma$ ).

To measure the delay between the continuum and line luminosity variations, it is a common practice in reverberation mapping studies to measure the monochromatic continuum fluxes in the vicinity of the reverberating lines. For the  $H\beta$  line it is the luminosity at 5100 Å, for the MgII line at 3000 Å, and for the CIV line at 1350 Å. Knowing these luminosities and a BLR radius–luminosity relation (Kaspi *et al.* 2000, 2007, Bentz *et al.* 2009), one can estimate the expected BLR radius and hence the central black hole mass.

Monochromatic luminosities can be turned into estimated time-lags for these lines, and may, for example, help in designing a spectroscopic experiment to observe them *via* spectroscopic (*e.g.*, Peterson 1993, Denney *et al.* 2010, Shen *et al.* 2015) or photometric (*e.g.*, Chelouche and Daniel 2012, Zu *et al.* 2013b) reverberation mapping. Inverting the problem, once a time-lag between a continuum flux and a reverberating line flux is measured, the absolute luminosity of an AGN is known, making it a “standardizable candle” (*e.g.*, Watson *et al.* 2011, Czerny *et al.* 2013).

Our main motivation here is to estimate the empirical monochromatic luminosities at these three rest-frame wavelengths (5100 Å, 3000 Å, 1350 Å) from the broad-band AGN magnitudes, when we lack flux-calibrated spectra or they are too noisy. We simply take the  $\approx 100\,000$  AGNs with spectroscopically measured monochromatic luminosities, black hole masses, emission lines, spectral slopes (Shen *et al.* 2011) and estimate the monochromatic fluxes based on the wealth of broad-band optical–IR magnitudes that are available (Schneider *et al.* 2010).

## 2. Data

To measure the monochromatic fluxes from the broad-band filters, we have downloaded the data for 105 783 quasars from Data Release 7 of SDSS from Schneider *et al.* (2010) and Shen *et al.* (2011). All of them are brighter than  $M_i < -22$  mag and have at least one broad emission line with a FWHM larger than 1000 km/s or interesting absorption features. Schneider *et al.* (2010) provide a dataset containing both the observed SDSS *ugriz* AB magnitudes for these objects as well as matched *JHK* and WISE magnitudes. We corrected these observed magnitudes for Galactic extinction using the extinction maps of Schlegel, Finkbeiner and Davis (1998). Schneider *et al.* (2010) already provide *u*-band extinction ( $A_u$ ) for all sources and we convert  $A_u$  to other wavelengths using the  $R_V = 3.1$  Galactic extinction curve (Cardelli, Clayton and Mathis 1989) with the

following values:  $A_g/A_u = 0.736$ ,  $A_r/A_u = 0.534$ ,  $A_i/A_u = 0.405$ ,  $A_z/A_u = 0.287$ ,  $A_U/A_u = 1.052$ ,  $A_V/A_u = 0.641$  (unused),  $A_R/A_u = 0.520$  (unused),  $A_I/A_u = 0.373$  (unused),  $A_J/A_u = 0.176$ ,  $A_H/A_u = 0.111$ ,  $A_K/A_u = 0.072$ ,  $A_{W1}/A_u = 0.033$ ,  $A_{W2}/A_u = 0.016$ ,  $A_{W3}/A_u = 0.000$ , and  $A_{W4}/A_u = 0.000$ . The extinctions in  $V$ ,  $R$ , and  $I$  bands were not used as these magnitudes were synthesized directly from the extinction-corrected  $ugriz$  magnitudes.

These quasars generally do not have the common Johnson-Cousins  $VRI$  magnitudes and we derive them directly from the extinction-corrected  $ugriz$  magnitudes. First, we calculate the  $r - R$ ,  $r - I$ ,  $i - R$  and  $i - I$  synthetic colors as a function of redshift using an average AGN spectrum from Richards *et al.* (2006a) and the respective filter transmission curves. We then match the SDSS dataset to the  $9 \text{ deg}^2$  AGN and Galaxy Evolution Survey (AGES; 152 AGN matches; Kochanek *et al.* 2012), containing  $R$  and  $I$  magnitudes, and shift the synthetic colors such that the converted  $R$  and  $I$  magnitudes match the ones observed in the NOAO Deep, Wide-Field Survey (NDWFS; Jannuzi and Dey 1999). We create  $R$  and  $I$  magnitudes from two sets of colors to verify their correctness (the dispersion is 0.12 mag).

While the NDWFS survey provides the  $RI$  magnitudes, it does not provide the  $V$ -band data. We therefore calculate the  $g - V$  synthetic colors as a function of redshift to obtain the  $V$ -band magnitudes and calibrate them with the observed  $V - I$  colors based on 758 quasars from the Magellanic Quasars Survey (Kozłowski *et al.* 2013), where the  $V$  and  $I$ -band magnitudes were provided by the OGLE sky survey (Udalski *et al.* 2008, Udalski, Szymański and Szymański 2015).

The extinction-corrected monochromatic luminosity at  $5100 \text{ \AA}$ ,  $3000 \text{ \AA}$  and  $1350 \text{ \AA}$  were already provided in Shen *et al.* (2011) for cosmological parameters  $H_0 = 70 \text{ (km/s)/Mpc}$ ,  $\Omega_M = 0.3$  and  $\Omega_\lambda = 0.7$ . We adopt the same cosmological parameters, hence our broad-band-to-monochromatic luminosity ratios are cosmological model-independent and can be used with any other set of cosmological parameters. One should be careful about using the low- $z$  ratios, as both the broad-band filters and the monochromatic luminosity can be affected by AGN host contamination.

### 3. Methodology

A broad-band luminosity  $L_F$  ( $\nu L_\nu$ ) in a filter  $F$  is calculated from

$$L_F = 4\pi D_L^2 \alpha_F \nu_F 10^{-0.4 \times m_F} \quad (1)$$

where  $L_F$  is in  $10^{23} \text{ erg/s}$ ,  $\alpha_F$  is the zero-magnitude flux [Jy] for a given filter  $F$  (column 3 in Table 1),  $m_F$  is the observed source magnitude,  $\nu_F$  is the central frequency [Hz] for that filter (column 4 in Table 1), and  $D_L$  is the luminosity distance [cm]. Details of the  $D_L$  calculation<sup>1</sup> from a redshift  $z$  and cosmological parameters are given in Wright (2006).

<sup>1</sup><http://www.astro.ucla.edu/~wright/CosmoCalc.html>

Table 1  
Basic properties of common astronomical filters

Filter	Central $\lambda$ [ $\mu\text{m}$ ]	flux at $m = 0$ [Jy]	Frequency [Hz]	Ref.
Galex				
FUV (Vega)	0.1539	514.98	$1.948 \times 10^{15}$	(1)
FUV (AB)	0.1539	3631.0	$1.948 \times 10^{15}$	(1)
NUV (Vega)	0.2316	781.84	$1.295 \times 10^{15}$	(1)
NUV (AB)	0.2316	3631.0	$1.295 \times 10^{15}$	(1)
UBVRI (Vega)				
U	0.375	1823.0	$7.994 \times 10^{14}$	(2)
B	0.430	4130.0	$6.972 \times 10^{14}$	(2)
V	0.554	3636.0	$5.414 \times 10^{14}$	(2)
R	0.641	3080.0	$4.677 \times 10^{14}$	(2)
I	0.789	2416.0	$3.802 \times 10^{14}$	(2)
SDSS (AB)				
u	0.3543	3631.0	$8.462 \times 10^{14}$	(3)
g	0.4770	3631.0	$6.285 \times 10^{14}$	(3)
r	0.6231	3631.0	$4.811 \times 10^{14}$	(3)
i	0.7625	3631.0	$3.932 \times 10^{14}$	(3)
z	0.9134	3631.0	$3.282 \times 10^{14}$	(3)
2MASS (Vega)				
J	1.235	1594.0	$2.427 \times 10^{14}$	(4)
H	1.662	1024.0	$1.804 \times 10^{14}$	(4)
K	2.159	666.7	$1.389 \times 10^{14}$	(4)
Spitzer (Vega)				
[3.6]	3.561	280.9	$8.419 \times 10^{13}$	(5)
[4.5]	4.509	179.7	$6.649 \times 10^{13}$	(5)
[5.8]	5.693	115.0	$5.266 \times 10^{13}$	(5)
[8.0]	7.982	64.13	$3.756 \times 10^{13}$	(5)
[24]	23.68	7.17	$1.265 \times 10^{13}$	(6)
[70]	71.42	0.778	$4.198 \times 10^{12}$	(7)
[160]	155.9	0.160	$1.923 \times 10^{12}$	(8)
WISE (Vega)				
W1	3.353	309.540	$8.850 \times 10^{13}$	(9)
W2	4.603	171.787	$6.445 \times 10^{13}$	(9)
W3	11.561	31.674	$2.675 \times 10^{13}$	(9)
W4	22.088	8.363	$1.346 \times 10^{13}$	(9)

In Column 2 the central wavelength of a filter is given, in Column 3 the flux [Jy] for an object of zero magnitude is given, and in Column 4 the corresponding frequency to the central wavelength of a filter is provided. References in Column 5 are: (1) Morrissey *et al.* (2007) – GALEX, (2) Bessell (1979) – *UBVRI*, (3) Oke and Gunn 1983, Fukugita *et al.* (1996) – SDSS, (4) Cohen, Wheaton and Megeath (2003) – 2MASS, (5) Reach *et al.* (2005) – IRAC, (6) Rieke *et al.* (2008) – MIPS 24  $\mu\text{m}$ , (7) Gordon *et al.* (2007) – MIPS 70  $\mu\text{m}$ , (8) Stansberry *et al.* (2007) – MIPS 160  $\mu\text{m}$ , and (9) Jarrett *et al.* (2011), Wright *et al.* (2010) – WISE.

Using the above prescription, we convert the extinction-corrected observed broad-band *ugriz*, *VRI* (converted), *JHK* and WISE magnitudes to the broad-band luminosities. We then calculate the empirical ratios  $R$  of the broad-band-to-monochromatic luminosity and provide their medians along with dispersions and uncertainties in 0.01 redshift bins (Table 2). They are also presented in Fig. 1. Note, that the ratios hold independent of the cosmological model.

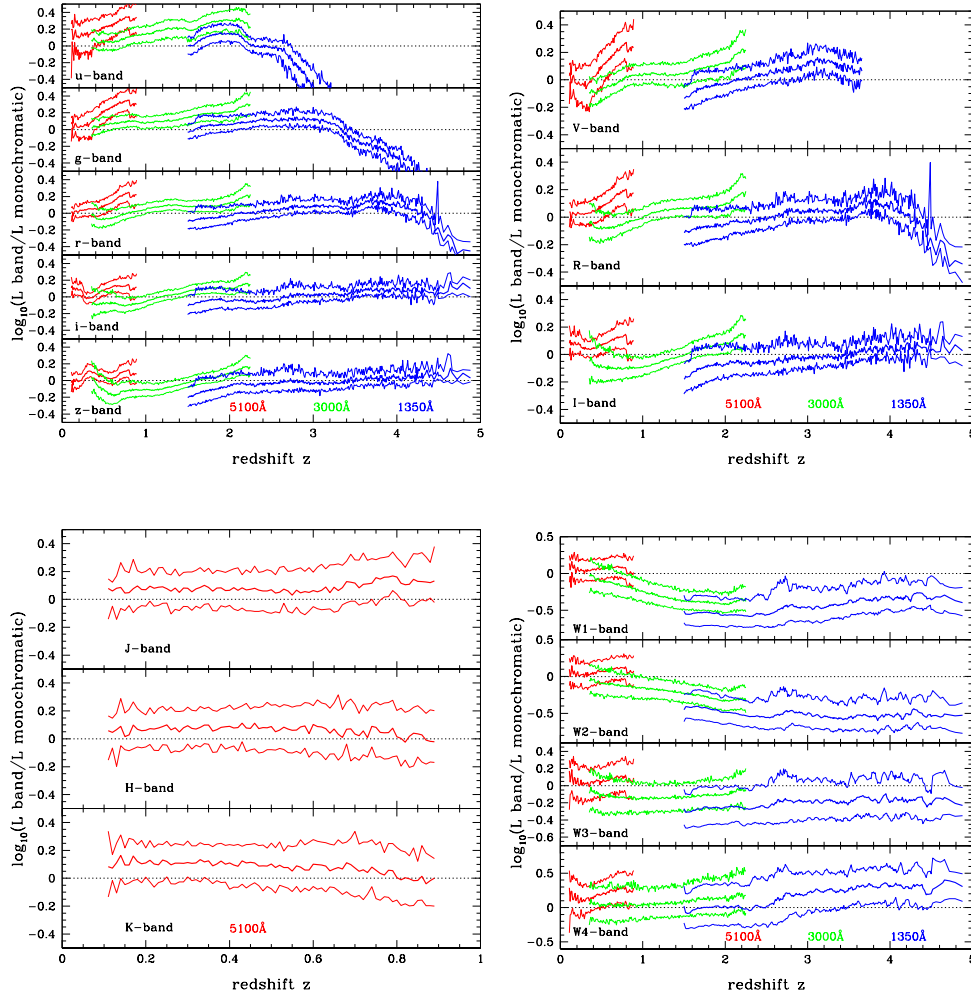


Fig. 1. Ratios between the broad-band SDSS *ugriz* (top-left panel), *VRI* (top-right), 2MASS *JHK* (bottom-left), and WISE (bottom-right) and monochromatic luminosity at 5100 Å (blue), 3000 Å (green) and 1350 Å (red). Both broad-band and monochromatic luminosity were derived with the same cosmological model, hence their ratios are model-independent. Having measured any of the magnitudes for an AGN at a redshift  $z$ , it is possible to convert that magnitude to either of three monochromatic luminosity with a typical dispersion of  $\approx 0.1$  dex. This may have profound implications for measurements of BLR radii and/or black hole masses.

Table 2

Median ratios between the broad-band and monochromatic luminosity

at 5100 Å							
$F$	$z$	$\log_{10}(R)$	$-\sigma$	$\sigma$	$-\text{err}$	$\text{err}$	$N_{\text{obj}}$
$u$	0.11	0.194	-0.582	0.066	-0.141	0.016	17
$u$	0.12	0.199	-0.151	0.106	-0.027	0.019	32
$u$	0.13	0.077	-0.149	0.142	-0.028	0.027	28
$u$	0.14	0.098	-0.272	0.131	-0.047	0.023	33
$u$	0.15	0.155	-0.113	0.224	-0.017	0.034	44
at 3000 Å							
$F$	$z$	$\log_{10}(R)$	$-\sigma$	$\sigma$	$-\text{err}$	$\text{err}$	$N_{\text{obj}}$
$u$	0.35	0.071	-0.085	0.125	-0.006	0.009	179
$u$	0.36	0.056	-0.089	0.114	-0.005	0.006	336
$u$	0.37	0.078	-0.101	0.104	-0.006	0.006	334
$u$	0.38	0.094	-0.123	0.103	-0.007	0.006	290
$u$	0.39	0.068	-0.096	0.117	-0.005	0.006	341
at 1350 Å							
$F$	$z$	$\log_{10}(R)$	$-\sigma$	$\sigma$	$-\text{err}$	$\text{err}$	$N_{\text{obj}}$
$u$	1.50	0.001	-0.094	0.091	-0.005	0.005	353
$u$	1.51	0.003	-0.103	0.114	-0.004	0.004	644
$u$	1.52	-0.002	-0.099	0.120	-0.004	0.005	574
$u$	1.53	0.011	-0.109	0.097	-0.005	0.004	511
$u$	1.54	0.001	-0.114	0.086	-0.004	0.003	717

$F$  is the broad-band filter,  $z$  is the redshift,  $\log_{10}(R)$  is the base 10 logarithm of the ratio between the band and monochromatic continuum luminosity,  $\sigma$  is the dispersion around the median value, and “err” is the uncertainty of the median ratio.

Full Table 2 is available in the electronic form from *Acta Astronomica Archive*. A portion is shown here for guidance regarding its form and content.

In addition to the tabular form, we also fit  $\log_{10}(R)$  as a simple function of redshift  $z$  with the formula

$$\log_{10}(R) = a + bz \quad (2)$$

in redshift ranges where this dependence is nearly linear. Typical dispersions between the best fits and the tabular data are  $\approx 0.02$  dex (*i.e.*, lower than the formal uncertainties from the tabular form). The best-fit values for selected redshift ranges are provided in Tables 3–4 and the residuals between the measured median ratios and the fitted ones are presented in Fig. 2.

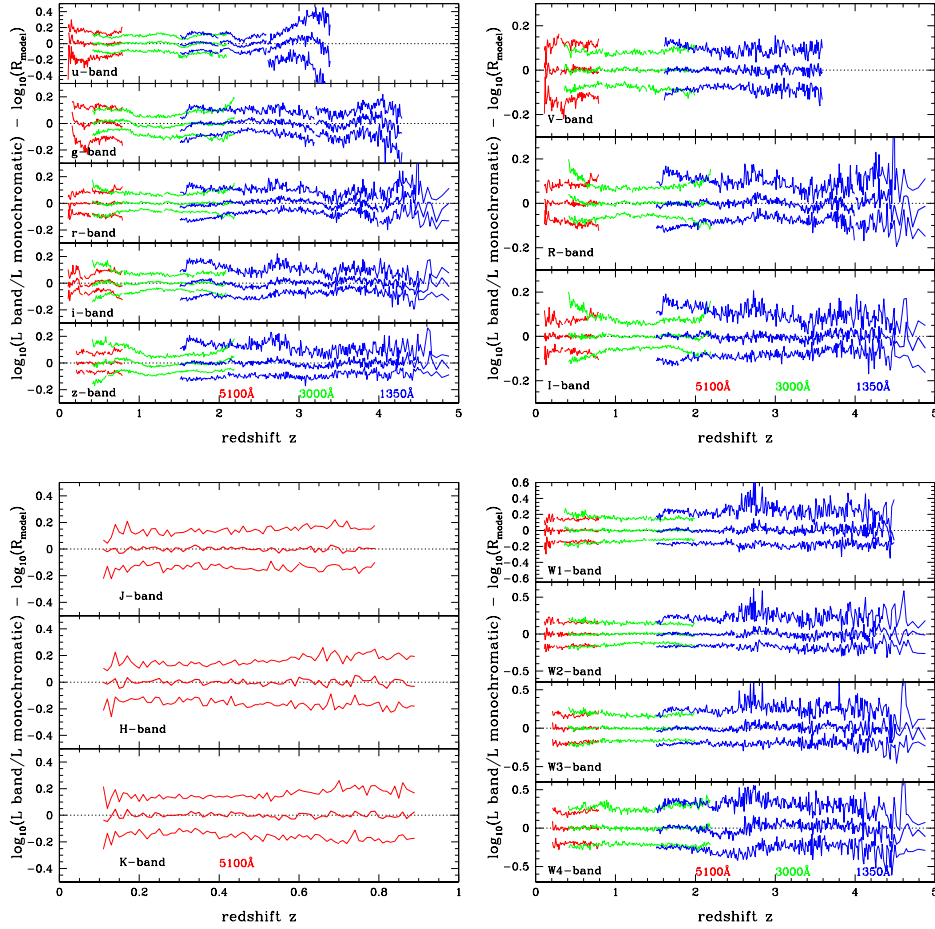


Fig. 2. Residuals after taking out the linear trends (Eq. 2) from the measured median ratios for the broad-band SDSS *ugriz* (top-left panel), *VRI* (top-right), 2MASS *JHK* (bottom-left), and WISE (bottom-right) and monochromatic luminosity at 5100 Å (blue), 3000 Å (green) and 1350 Å (red).

A desired monochromatic luminosity can be estimated from

$$\log_{10}(\lambda L_{\lambda}) = \log_{10}(L_F) - \log_{10}(R) \quad (3)$$

where  $\log_{10}(L_F)$  is estimated from Eq.(1) and  $\log_{10}(R)$  is provided either in Table 2 or parametric form from Eq.(2) with the fitted values stored in Tables 3–4.

#### 4. A Simple Prescription

Imagine a situation when one knows that the source is an AGN but its spectrum is not flux-calibrated or its signal-to-noise (S/N) is too low to reliably measure its monochromatic luminosity. What one has at hand are just its broad-band common magnitudes and the redshift estimate.

Table 3

Best-fit parameters to Eq.(2) for optical bands

$F$	$\lambda_{\text{cont.}}$	$z$ range	$a$	$\sigma_a$	$b$	$\sigma_b$
$u$	5100 Å	0.1–0.8	0.019	0.006	0.405	0.011
$g$	5100 Å	0.15–0.8	−0.107	0.006	0.613	0.013
$r$	5100 Å	0.1–0.4	0.002	0.005	0.142	0.017
$r$	5100 Å	0.4–0.8	−0.194	0.008	0.562	0.012
$i$	5100 Å	0.1–0.3	0.212	0.019	−0.719	0.093
$i$	5100 Å	0.3–0.8	−0.111	0.010	0.352	0.018
$z$	5100 Å	0.2–0.32	−0.271	0.019	1.245	0.074
$z$	5100 Å	0.32–0.59	0.231	0.009	−0.373	0.019
$z$	5100 Å	0.59–0.8	−0.323	0.020	0.578	0.029
$u$	3000 Å	0.4–2.1	−0.037	0.003	0.175	0.002
$g$	3000 Å	0.4–2.2	−0.020	0.004	0.120	0.003
$r$	3000 Å	0.4–1.3	−0.178	0.003	0.222	0.003
$r$	3000 Å	1.3–1.9	0.106	0.008	−0.013	0.005
$r$	3000 Å	1.9–2.2	−0.654	0.036	0.389	0.017
$i$	3000 Å	0.4–0.8	−0.051	0.010	−0.057	0.016
$i$	3000 Å	0.8–1.7	−0.279	0.004	0.229	0.003
$i$	3000 Å	1.7–2.2	−0.050	0.024	0.083	0.012
$z$	3000 Å	0.4–0.6	0.316	0.021	−0.852	0.045
$z$	3000 Å	0.6–2.2	−0.299	0.005	0.190	0.003
$u$	1350 Å	1.5–2.0	−0.513	0.032	0.348	0.018
$u$	1350 Å	2.0–2.6	0.810	0.047	−0.337	0.020
$u$	1350 Å	2.6–3.4	4.295	0.113	−1.616	0.038
$g$	1350 Å	1.5–3.2	−0.074	0.009	0.068	0.004
$g$	1350 Å	3.2–4.3	1.961	0.049	−0.587	0.013
$r$	1350 Å	1.5–4.0	−0.188	0.006	0.083	0.002
$r$	1350 Å	4.0–4.9	2.985	0.156	−0.705	0.036
$i$	1350 Å	1.5–4.9	−0.165	0.005	0.060	0.002
$z$	1350 Å	1.5–2.1	−0.576	0.012	0.259	0.007
$z$	1350 Å	2.1–4.9	−0.149	0.007	0.045	0.002
$V$	5100 Å	0.1–0.3	0.062	0.017	−0.381	0.081
$V$	5100 Å	0.3–0.8	−0.249	0.006	0.667	0.011
$R$	5100 Å	0.1–0.35	0.017	0.009	0.030	0.040
$R$	5100 Å	0.35–0.8	−0.128	0.006	0.415	0.010
$I$	5100 Å	0.1–0.35	0.118	0.007	−0.234	0.030
$I$	5100 Å	0.35–0.8	−0.057	0.004	0.255	0.006
$V$	3000 Å	0.35–0.85	−0.199	0.006	0.263	0.009
$V$	3000 Å	0.85–1.4	0.035	0.006	0.002	0.006
$V$	3000 Å	1.4–2.0	−0.175	0.006	0.149	0.003
$R$	3000 Å	0.4–1.2	−0.195	0.004	0.196	0.004
$R$	3000 Å	1.2–1.9	0.007	0.004	0.036	0.003
$R$	3000 Å	1.9–2.2	−0.580	0.036	0.339	0.017
$I$	3000 Å	0.4–0.9	−0.072	0.005	−0.036	0.008
$I$	3000 Å	0.9–2.2	−0.275	0.003	0.182	0.018
$V$	1350 Å	1.6–3.2	−0.301	0.005	0.138	0.002
$V$	1350 Å	3.2–3.6	0.778	0.083	−0.199	0.024
$R$	1350 Å	1.5–4.0	−0.218	0.004	0.084	0.002
$R$	1350 Å	4.0–4.9	2.009	0.092	−0.479	0.022
$I$	1350 Å	1.5–1.8	−0.671	0.028	0.333	0.017
$I$	1350 Å	1.8–4.9	−0.182	0.005	0.054	0.002



Table 4

Best-fit parameters to Eq.(2) for infrared bands

$F$	$\lambda_{\text{cont.}}$	$z$ range	$a$	$\sigma_a$	$b$	$\sigma_b$
$J$	5100 Å	0.1–0.6	0.085	0.005	−0.042	0.014
$J$	5100 Å	0.6–0.8	−0.313	0.051	0.603	0.073
$H$	5100 Å	0.1–0.5	0.051	0.008	0.081	0.025
$H$	5100 Å	0.5–0.9	0.184	0.026	−0.196	0.037
$K$	5100 Å	0.1–0.7	0.128	0.006	−0.071	0.015
$K$	5100 Å	0.7–0.9	0.422	0.066	−0.503	0.082
$W1$	5100 Å	0.1–0.25	0.191	0.042	−0.655	0.232
$W1$	5100 Å	0.25–0.8	0.007	0.006	0.112	0.010
$W2$	5100 Å	0.1–0.25	0.127	0.046	−0.460	0.258
$W2$	5100 Å	0.25–0.8	−0.040	0.006	0.217	0.012
$W3$	5100 Å	0.2–0.8	−0.022	0.008	0.162	0.015
$W4$	5100 Å	0.2–0.8	0.013	0.008	0.361	0.016
$W1$	3000 Å	0.35–1.4	0.054	0.003	−0.295	0.004
$W1$	3000 Å	1.4–2.0	−0.242	0.010	−0.085	0.006
$W2$	3000 Å	0.4–2.0	−0.005	0.002	−0.152	0.002
$W3$	3000 Å	0.4–0.8	−0.030	0.012	−0.146	0.020
$W3$	3000 Å	0.8–2.0	−0.186	0.004	0.039	0.003
$W4$	3000 Å	0.4–0.7	0.080	0.022	−0.071	0.040
$W4$	3000 Å	0.7–2.2	−0.058	0.006	0.100	0.003
$W1$	1350 Å	1.5–2.5	−0.488	0.013	−0.033	0.006
$W1$	1350 Å	2.5–4.5	−0.846	0.026	0.127	0.007
$W2$	1350 Å	1.5–2.5	−0.131	0.011	−0.174	0.005
$W2$	1350 Å	2.5–4.9	−0.511	0.021	−0.005	0.006
$W3$	1350 Å	1.5–4.9	−0.338	0.010	0.044	0.003
$W4$	1350 Å	1.5–4.9	−0.274	0.014	0.146	0.005

2MASS detections are limited to  $z < 0.8$  sources therefore the measurement of conversions to monochromatic luminosities at 3000 Å and 1350 Å is not feasible.

As an example, let assume we are interested in obtaining the monochromatic luminosity for a quasar SDSS J000006.53+003055.2 at (RA, Decl.) = (0.027228, 0.551534) deg at a redshift of  $z = 1.8246$ . It is drawn from the sample analyzed in the paper, hence the true spectral monochromatic luminosity is known. Its extinction-corrected magnitudes are  $u = 20.254 \pm 0.065$  mag,  $g = 20.365 \pm 0.034$  mag,  $r = 20.255 \pm 0.038$  mag,  $i = 20.040 \pm 0.041$  mag,  $z = 20.005 \pm 0.121$  mag,  $V = 20.431$  mag (estimated),  $R = 20.067$  mag (estimated),  $I = 19.661$  mag (estimated),  $JHK$  not measured,  $W1 = 16.560 \pm 0.084$  mag,  $W2 = 15.094 \pm 0.093$  mag,  $W3 = 12.549 \pm 0.539$  mag, and  $W4 = 8.072$  mag.

The broad-band luminosities [erg/s], are then  $\log_{10}(L_u) = 45.748 \pm 0.026$ ,  $\log_{10}(L_g) = 45.583 \pm 0.014$ ,  $\log_{10}(L_r) = 45.508 \pm 0.015$ ,  $\log_{10}(L_i) = 45.510 \pm 0.016$ ,  $\log_{10}(L_z) = 45.447 \pm 0.048$ ,  $\log_{10}(L_V) = 45.485$ ,  $\log_{10}(L_R) = 45.495$ ,

$\log_{10}(L_I) = 45.462$ ,  $\log_{10}(L_{W1}) = 45.177 \pm 0.034$ ,  $\log_{10}(L_{W2}) = 45.370 \pm 0.037$ ,  $\log_{10}(L_{W3}) = 45.271 \pm 0.216$ , and  $\log_{10}(L_{W4}) = 46.185$ .

From Fig. 1, it is clear that at this redshift it is possible to derive both 3000 Å and 1350 Å luminosity from the broad-band filters. Table 5 gives the derived values. In this particular case, the optical bands seem to reproduce the real values better (to within  $\approx 1\sigma$ ) than the infrared ones. The overestimate of the luminosity from the infrared filters may be attributed to the host contamination, as galaxies are usually much brighter in infrared than in visible light.

Table 5

Example of monochromatic luminosity estimates for AGN SDSS J000006.53+003055.2

filter	$\log_{10}(R)$	$\log_{10}(\lambda L_{\lambda}/\text{erg/s})$ at 3000 Å	$\log_{10}(R)$	$\log_{10}(\lambda L_{\lambda}/\text{erg/s})$ at 1350 Å
spec.	...	$45.32 \pm 0.04$	...	$45.60 \pm 0.03$
<i>u</i>	0.30	$45.45 \pm 0.12$	0.14	$45.61 \pm 0.11$
<i>g</i>	0.20	$45.38 \pm 0.09$	0.05	$45.53 \pm 0.10$
<i>r</i>	0.09	$45.42 \pm 0.07$	-0.06	$45.57 \pm 0.11$
<i>i</i>	0.11	$45.40 \pm 0.07$	-0.04	$45.55 \pm 0.12$
<i>z</i>	0.04	$45.41 \pm 0.07$	-0.11	$45.56 \pm 0.13$
<i>V</i>	0.10	$45.39 \pm 0.09$	-0.05	$45.54 \pm 0.10$
<i>R</i>	0.08	$45.42 \pm 0.07$	-0.07	$45.57 \pm 0.11$
<i>I</i>	0.06	$45.40 \pm 0.07$	-0.08	$45.54 \pm 0.12$
W1	-0.40	$45.58 \pm 0.13$	-0.54	$45.72 \pm 0.20$
W2	-0.29	$45.66 \pm 0.14$	-0.45	$45.82 \pm 0.19$
W3	-0.11	$45.38 \pm 0.16$	-0.28	$45.55 \pm 0.20$
W4	0.14	$46.05 \pm 0.28$	0.00	$46.19 \pm 0.30$

## 5. Discussion

AGN are well known as variable sources (see Ulrich, Maraschi and Urry 1997 for a review). Their variability is aperiodic and well-modeled by the damped random walk method (*e.g.*, Kelly, Bechtold and Siemiginowska 2009, Kozłowski *et al.* 2010a, Zu *et al.* 2013a). A simplified description of their variability is *via* the structure function – a quantity that measures the average magnitude difference for a time difference between any two epochs (*e.g.*, Schmidt *et al.* 2010). It is described by

$$SF(\tau) = SF_0 \left( \frac{\tau}{\tau_0} \right)^\gamma \quad (4)$$

where  $SF_0$  is the structure function at a fixed  $\tau_0$ ,  $\tau$  is the time difference between two observations, and  $\gamma$  is the slope of the structure function.

Because both the broad-band optical or infrared observations and the spectra were taken at different epochs, usually a few years apart, a fraction of the scatter in the derived ratios is due to variability itself and not the intrinsic differences between AGNs. Collecting information on the time differences between all observations is beyond the scope of this paper, nevertheless we roughly estimate the imprint of variability contribution to the scatter in the relations.

Most SDSS observations investigated here, both spectroscopic and photometric, were obtained in the years 2000–2010, as were the WISE observations. Only the 2MASS data were obtained earlier. For an order of magnitude estimate, we assume that the median difference between any two observations is five years, and we know from the sample that the median AGN redshift is  $z \approx 1.5$ . This means that the median rest-frame time difference is five years times  $(1+z)^{-1}$ , hence two years.

Vanden Berk *et al.* (2004) measured the *gri* structure function parameters for 25 000 SDSS quasars with approximately  $\tau_0 = 2$  years,  $SF_0 = 0.28$  mag and  $\gamma = 0.30$ . Since our median rest-frame time difference is two years and both the broad-band and monochromatic light curves are highly correlated, we can expect the median change in  $\log_{10}(R)$  to be of order of 0.1 dex. This implies that this variability is responsible for a significant fraction of the dispersions reported in this paper.

Kozłowski *et al.* (2010b, 2015) analyzed the variability of  $\approx 1500$  quasars observed by the Spitzer Space Telescope at  $3.6 \mu\text{m}$  and  $4.5 \mu\text{m}$  (bands nearly identical to the *W1* and *W2* WISE bands, respectively), and found for the rest-frame  $\tau_0 = 2$  years  $SF_0 = 0.12$  mag and  $\gamma = 0.47$  for  $3.6 \mu\text{m}$  and  $SF_0 = 0.13$  mag and  $\gamma = 0.45$  for  $4.5 \mu\text{m}$ . Again, we estimate the expected median variance between the optical and IR bands in  $\log_{10}(R)$  is  $< 0.1$  dex.

It is clear that such intrinsic AGN parameters as the black hole mass, emission lines strength and width, spectrum shape, or the host contamination will have impact on the derived ratios. In Fig. 3, we inspect the dependence of the derived ratios on the emission line width (top-left panel), its strength (top-right panel), the black hole mass (bottom-left panel), and the spectral slope (bottom-right panel) using the estimates from Shen *et al.* (2011). As an example, we use the conversion from the *r*-band to monochromatic luminosity at  $3000 \text{ \AA}$  and the MgII line parameters for the  $z = 0.4\text{--}2.1$  quasars. From Fig. 3, we see that there is little or no dependence of  $\log_{10}(R)$  as the MgII line width and strength or the black hole mass. There is a hint of weak anti-correlations with  $\log_{10}(R)$  for the latter two observables, but they are most prominent at the redshift extremes, where there are less objects per bin, and the ratios are less precisely determined. There is, as expected, correlation with the continuum slope. Over 91% of AGNs have slopes in the range  $-2 < \text{slope} < 0$ , while the ratio changes by up to  $1\sigma$  inside the entire redshift range between  $-2 < \text{slope} < -1$  and  $-1 < \text{slope} < 0$ . The ratios for AGNs with  $0 < \text{slope} < 2$  seem not to follow the ones from the main sample, they, however, constitute only 2% of the sample.

The BLR radius-relation is  $r \propto L^{1/2}$ , so the black hole mass scales as  $M_{BH} \propto L^{1/2}v^2$ . Keeping the BLR velocity fixed, an 0.1 dex change in luminosity introduces  $\approx 12\%$  change in radius and/or black hole mass. These unlucky 2% of AGNs with  $0 < \text{slope} < 2$  will introduce additional biases of that order in the black hole mass or BLR radius estimate.

We note that these luminosity conversions are based on a large sample of ‘‘average’’ quasars. There are some residual correlations but they appear to introduce typical shift of 0.1 dex – a minor price to pay if the spectrum for the object does not exist, is of low quality, or it is not feasible to determine the continuum slope.

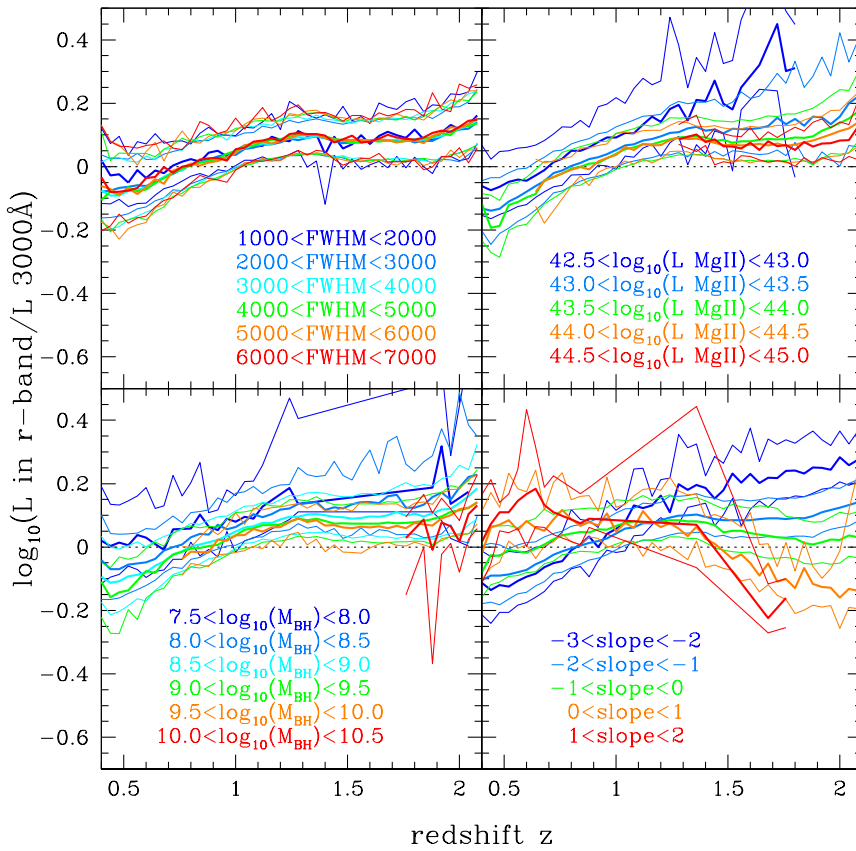


Fig. 3. Correlations between the measured median ratios of the  $r$ -band to  $3000 \text{ \AA}$  luminosity with the MgII emission line width and strength, black hole mass, and the spectral slope. There is no obvious correlation with the MgII FWHM (expressed here in km/s), but there is a weak hint of anticorrelation with the MgII strength (in erg/s) and the black hole mass (in  $M_{\odot}$ ). There is, however, a strong correlation of the ratios with the continuum slope, and changing with redshift. We note that over 91% of quasars have the slope in a range  $-2 < \text{slope} < 0$  (green–light-blue). The AGNs with  $-2 < \text{slope} < -1$  and  $-1 < \text{slope} < 0$  have ratios different by at most  $1\sigma$  or 0.1 dex across the entire redshift range. While the ratios for AGNs with  $0 < \text{slope} < 2$  (orange–red) do not follow the ones for the main sample, they constitute only 2% of the sample.

## 6. Summary

In this paper, we have been interested in empirical conversions of broad-band AGN magnitudes to the monochromatic luminosities that are essential in calculating the bolometric AGN luminosity, central black hole mass *via* the radius–luminosity relation, or simply the BLR radius. Using the 105 783 SDSS DR7 quasars, we calculate the ratios between AGN luminosities as observed in common astronomical filters and their monochromatic luminosity as a function of redshift. We provide a simple prescription for using the broad-band magnitudes to calculate monochromatic luminosity at 5100 Å, 3000 Å, and 1350 Å.

AGNs do have different spectral shapes and different contributions from the emission lines, hence the median values derived and provided in this paper should rather serve as “best estimates” and not as “measurements”. Ratios for low redshift AGNs with  $z < 0.5$  may also be affected by AGN host contamination, and hence are less reliable than the estimates at higher redshifts. Galaxies are brightest in infrared, therefore the infrared estimates (2MASS, WISE) should be used with even higher caution, as shown in the discussed example above. We also study correlations of derived conversions with the black hole mass, emission lines strength and width, and the spectrum slope. Only the latter has a noticeable impact (of up to  $\approx 0.1$  dex) on the derived conversions, but in the absence of spectrum or when the spectrum is of low quality, this is a low price to pay for a monochromatic luminosity estimate.

Since the majority of observations were taken at significantly different epochs, we estimate that a fair fraction of the reported uncertainties is not related to the intrinsic AGN properties, but simply due to variability.

Having the broad-band magnitudes converted to any or all the monochromatic luminosities, it is straightforward to estimate the BLR radius using the BLR-radius–luminosity relation (Kaspi *et al.* 2000, Bentz *et al.* 2009). Transformations provided in this paper may also serve as tools in designing future spectroscopic and/or photometric reverberation mapping campaigns, similar to the one reported in Shen *et al.* (2015).

Bolometric luminosities ( $L_{\text{bol}}$ ) are an important diagnostic for AGN studies, as they are necessary in calculating the Eddington ratio ( $= L_{\text{bol}}/L_{\text{Edd}}$ , where  $L_{\text{Edd}} = 1.26 \times 10^{38} (M_{\text{BH}}/M_{\odot})$  erg/s), and what follows, the mass accretion rate (see *e.g.*, Peterson 1997). Bolometric luminosities of AGNs can be calculated from their monochromatic luminosities, where these fluxes are “simply multiplied” by 9.26, 5.15, and 3.18 for 5100 Å, 3000 Å, and 1350 Å (see discussion in Shen *et al.* 2011 and/or Richards *et al.* 2006b). Here, they can be estimated by adding 0.97, 0.71, and 0.50 in Eq.(3), respectively.

We provide a simple online calculator of monochromatic and bolometric AGN luminosities based on the analytic conversions from Eqs.(2–3) and Tables 3 and 4:

<http://www.astro.uw.edu.pl/~simkoz/AGNcalc>

**Acknowledgements.** This work has been supported by the Polish National Science Centre grant No. 2014/15/B/ST9/00093. We thank Prof. Christopher S. Kochanek for careful reading of the manuscript and many comments that helped to improve it. We also thank Dr. Kelly Denney for helpful comments on the manuscript. This research has made use of the SIMBAD database, operated at CDS, Strasbourg, France. This research has made use of the NASA/IPAC Extragalactic Database (NED) which is operated by the Jet Propulsion Laboratory, California Institute of Technology, under contract with the National Aeronautics and Space Administration.

## REFERENCES

- Bentz, M.C., Peterson, B.M., Netzer, H., Pogge, R.W., and Vestergaard, M. 2009, *ApJ*, **697**, 160.
- Bessell, M.S. 1979, *PASP*, **91**, 589.
- Cardelli, J.A., Clayton, G.C., and Mathis, J.S. 1989, *ApJ*, **345**, 245.
- Chelouche, D., and Daniel, E. 2012, *ApJ*, **747**, 62.
- Cohen, M., Wheaton, W.A., and Megeath, S.T. 2003, *AJ*, **126**, 1090.
- Collier, S.J., *et al.* 1998, *ApJ*, **500**, 162.
- Czerny, B., Hryniewicz, K., Maity, I., Schwarzenberg-Czerny, A., Życki, P.T., and Bilicki, M. 2013, *A&A*, **556**, A97.
- Denney, K.D., *et al.* 2010, *ApJ*, **721**, 715.
- Fukugita, M., Ichikawa, T., Gunn, J.E., Doi, M., Shimasaku, K., and Schneider, D.P. 1996, *AJ*, **111**, 1748.
- Gordon, K.D., *et al.* 2007, *PASP*, **119**, 1019.
- Jannuzi, B.T., and Dey, A. 1999, in: "Photometric Redshifts and the Detection of High Redshift Galaxies", *ASP Conference Series*, **191**, p.111.
- Jarrett, T.H., *et al.* 2011, *ApJ*, **735**, 112.
- Kaspi, S., Smith, P.S., Netzer, H., Maoz, D., Jannuzi, B.T., and Giveon, U. 2000, *ApJ*, **533**, 631.
- Kaspi, S., Brandt, W.N., Maoz, D., *et al.* 2007, *ApJ*, **659**, 997.
- Kelly, B.C., Bechtold, J., and Siemiginowska, A. 2009, *ApJ*, **698**, 895.
- Kochanek, C.S., *et al.* 2012, *ApJS*, **200**, 8.
- Kozłowski, S., *et al.* 2010a, *ApJ*, **708**, 927.
- Kozłowski, S., *et al.* 2010b, *ApJ*, **716**, 530.
- Kozłowski, S., *et al.* 2013, *ApJ*, **775**, 92.
- Kozłowski, S., Kochanek, C.S., Ashby, M.L.N., Assef, R.J., Brodwin, M., Eisenhardt, P.R., Jannuzi, B.T., and Stern, D. 2015, arXiv:1509.02467.
- Morrissey, P., *et al.* 2007, *ApJS*, **173**, 682.
- Oke, J.B., and Gunn, J.E. 1983, *ApJ*, **266**, 713.
- Peterson, B.M. 1993, *PASP*, **105**, 247.
- Peterson, B.M. 1997, "An introduction to active galactic nuclei", Cambridge, New York Cambridge University Press.
- Reach, W.T., *et al.* 2005, *PASP*, **117**, 978.
- Richards, G.T., *et al.* 2006a, *AJ*, **131**, 2766.
- Richards, G.T., *et al.* 2006b, *ApJS*, **166**, 470.
- Rieke, G.H., *et al.* 2008, *AJ*, **135**, 2245.
- Shakura, N.I., and Sunyaev, R.A. 1973, *A&A*, **24**, 337.
- Schlegel, D.J., Finkbeiner, D.P., and Davis, M. 1998, *ApJ*, **500**, 525.
- Schmidt, K.B., Marshall, P.J., Rix, H.-W., Jester, S., Hennawi, J.F., and Dobler, G. 2010, *ApJ*, **714**, 1194.
- Schneider, D.P., *et al.* 2010, *AJ*, **139**, 2360.

- Shen, Y., *et al.* 2011, *ApJS*, **194**, 45.  
Shen, Y., *et al.* 2015, *ApJS*, **216**, 4.  
Stansberry, J.A., *et al.* 2007, *PASP*, **119**, 1038.  
Udalski, A., Szymański, M.K., Soszyński, I., and Poleski, R. 2008, *Acta Astron.*, **58**, 69.  
Udalski, A., Szymański, M.K., and Szymański, G. 2015, *Acta Astron.*, **65**, 1.  
Ulrich, M.-H., Maraschi, L., and Urry, C.M. 1997, *Ann. Rev. Astron. Astrophys.*, **35**, 445.  
Vanden Berk, D.E., *et al.* 2004, *ApJ*, **601**, 692.  
Vestergaard, M., and Peterson, B.M. 2006, *ApJ*, **641**, 689.  
Watson, D., Denney, K.D., Vestergaard, M., and Davis, T.M. 2011, *ApJ*, **740**, L49.  
Wright, E.L. 2006, *PASP*, **118**, 1711.  
Wright, E.L., *et al.* 2010, *AJ*, **140**, 1868.  
Zu, Y., Kochanek, C.S., Kozłowski, S., and Udalski, A. 2013, *ApJ*, **765**, 106.  
Zu, Y., Kochanek, C.S., Kozłowski, S., and Peterson, B.M. 2013, arXiv:1310.6774.